

# G3Flow: Generative 3D Semantic Flow for Pose-aware and Generalizable Object Manipulation

Tianxing Chen<sup>1,2,3\*</sup> Yao Mu<sup>1\*†</sup> Zhixuan Liang<sup>1\*</sup> Zanxin Chen<sup>3,4</sup> Shijia Peng<sup>3,4</sup>  
Qiangyu Chen<sup>3</sup> Mingkun Xu<sup>5</sup> Ruizhen Hu<sup>3</sup> Hongyuan Zhang<sup>1,2</sup> Xuelong Li<sup>2</sup> Ping Luo<sup>1†</sup>

<sup>1</sup>The University of Hong Kong <sup>2</sup>Institute of Artificial Intelligence (TeleAI), China Telecom  
<sup>3</sup>Shenzhen University <sup>4</sup>AgileX Robotics <sup>5</sup>Guangdong Institute of Intelligence Science and Technology

<https://tianxingchen.github.io/G3Flow>

## Abstract

Recent advances in imitation learning for 3D robotic manipulation have shown promising results with diffusion-based policies. However, achieving human-level dexterity requires seamless integration of geometric precision and semantic understanding. We present **G3Flow**, a novel framework that constructs real-time semantic flow, a dynamic, object-centric 3D semantic representation by leveraging foundation models. Our approach uniquely combines 3D generative models for digital twin creation, vision foundation models for semantic feature extraction, and robust pose tracking for continuous semantic flow updates. This integration enables complete semantic understanding even under occlusions while eliminating manual annotation requirements. By incorporating semantic flow into diffusion policies, we demonstrate significant improvements in both terminal-constrained manipulation and cross-object generalization. Extensive experiments across five simulation tasks show that G3Flow consistently outperforms existing approaches, achieving up to 68.3% and 50.1% average success rates on terminal-constrained manipulation and cross-object generalization tasks respectively. Our results demonstrate the effectiveness of G3Flow in enhancing real-time dynamic semantic feature understanding for robotic manipulation policies.

## 1. Introduction

Recent years have witnessed significant advances in imitation learning for robotic manipulation, leading to remarkable achievements across various tasks [1, 5, 15, 16, 40]. Image-based imitation learning methods often face challenges in precise manipulation and sample efficiency due to

\*Co-first authors. Equal contribution.

†Corresponding authors. Contact {ymu, pluo}@cs.hku.hk

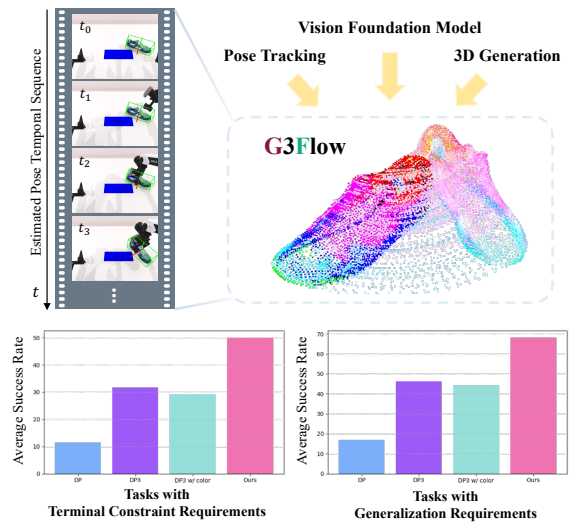


Figure 1. **Overview of G3Flow.** Our approach leverages the 3D generative model and language-guided object detection model to generate 3D semantic flow (top). Through continuous tracking-based updates, G3Flow enables pose-aware and generalizable manipulation, demonstrating superior performance in multiple challenging 3D manipulation tasks (bottom), with significant improvements over baselines (DP, DP3, and DP3 w/ color).

their limited ability to capture geometric relationships. In parallel, researchers have developed 3D imitation learning methods utilizing point clouds [4, 10, 39] or voxel [6, 29] representations, which enhanced few-shot learning capabilities by capturing geometric information. Among these approaches, 3D diffusion-based policies [10, 39] have shown promising results across multiple robotic tasks, owing to their superior ability to model multi-modal distributions. However, these geometry-centric methods, despite their advantages, often lack the crucial semantic understanding necessary for sophisticated manipulation tasks. For instance, in pose-aware manipulation scenarios such as shoe placement or tool organization, purely geometric representations struggle to identify semantically meaningful parts (such as

the toe of a shoe) or handle cases where semantically similar objects exhibit significant geometric variations. This limitation highlights a critical research direction: the integration of rich semantic information from 2D images with geometric features from 3D representations. Such integration is essential for advancing performance in tasks that demand both precise spatial control and semantic comprehension, potentially bridging the gap between geometric precision and semantic understanding in robotic manipulation.

Several approaches have recently emerged to address this semantic understanding challenge in robotic manipulation. D<sup>3</sup>Fields [34] introduced dynamic 3D descriptor fields, while subsequent works like GenDP [33] explored category-level generalization through semantic fields. However, these methods face significant practical challenges: they require manual annotation of reference objects and struggle with maintaining semantic consistency during dynamic interactions. Specifically, occlusions during manipulation not only result in incomplete object observations but also pose significant challenges to feature acquisition, severely affecting semantic understanding and limiting their real-world applicability.

In this paper, we propose G3Flow, a novel foundation model-driven approach that constructs real-time semantic flow, a dynamic, object-centric, and complete 3D semantic representation that maintains consistency even under occlusions. Our key insight is to leverage the complementary capabilities of foundation models: 3D generative models create precise digital twins from multi-view observations, vision foundation models extract rich semantic features, and robust pose tracking models enable continuous semantic flow updates. This combination eliminates manual annotation while ensuring persistent semantic understanding throughout the manipulation process. Specifically, our framework operates in two phases: (1) Initial semantic field establishment through object-centric exploration and 3D object generation, where a robot actively gathers multi-view observations to create a comprehensive digital twin and its base semantic field; and (2) Semantic flow generation through real-time pose tracking, which continuously transforms the semantic field to create a dynamic flow that aligns with the physical object during manipulation, maintaining completeness even under occlusions. This semantic flow serves as a powerful enhancement for downstream manipulation policies, enabling them to better handle both precise control tasks and object variations.

Through extensive experiments on both terminal-constrained manipulation and cross-object generalization tasks, we demonstrate that policy with G3Flow significantly outperforms existing methods, achieving up to 68.3% v.s. 46.2% and 50.1% v.s. 31.7% success rates comparing to next best method on these two tasks. Our approach achieves superior success rates in precise manip-

ulation tasks and shows strong generalization capabilities across object variants, validating the effectiveness of our semantic flow framework. These results demonstrate the potential of enhancing imitation learning policies with rich semantic representations, paving the way for more precise and generalizable robotic manipulation.

Our key contributions can be summarized as follows: (1) We propose a novel foundation model-driven approach for constructing semantic flow, a dynamic and complete semantic representation through the integration of 3D generation, detection, and pose tracking models, enabling real-time understanding robust to occlusions without manual annotation. (2) We develop a semantic flow-based imitation learning framework that leverages the dynamic semantic representation for enhanced manipulation, enabling both precise terminal control and effective generalization across object variations. (3) Through extensive experimental validation, we demonstrate that our semantic flow significantly enhances imitation learning policies, achieving up to 68.3% and 50.1% success rates on terminal-constrained tasks and cross-object generalization respectively.

## 2. Related Work

### 2.1. 3D Semantic Fields for Robotics Manipulation

Semantic fields have emerged as a promising direction for enhancing robotic manipulation by providing a rich semantic understanding of the environment [24, 28, 33, 34]. These approaches aim to bridge the gap between geometric perception and semantic comprehension, which is crucial for advanced manipulation capabilities.

D<sup>3</sup>Fields[34] pioneered the integration of dynamic 3D descriptor fields for manipulation, while subsequent works further expanded the potential of semantic fields. OVMM[24] explored open-vocabulary mobile manipulation through vision-language models, GenDP[33] addressed category-level generalization in diffusion policies, and F3RM[28] enabled natural language specification through CLIP-based semantic distillation.

However, fundamental challenges remain in obtaining and maintaining reliable semantic fields for robotic manipulation. Current approaches like D<sup>3</sup>Fields[34] and GenDP[33] heavily rely on manual annotation of reference objects and face significant challenges during object interactions. Specifically, occlusions not only result in incomplete object observations but also pose significant challenges to feature acquisition, severely affecting semantic understanding during manipulation. These limitations underscore the need for a paradigm shift in how semantic fields are constructed and maintained during manipulation tasks - a challenge that our work addresses through a novel foundation model-driven approach that enables dynamic, object-centric, and complete 3D semantic fields in real-time

under closed-loop control.

## 2.2. 3D Generative Models for Robotics Simulation

Recent advances in 3D object generation have witnessed various foundational models employing different technical approaches. Early attempts like GET3D [3] leveraged generative adversarial networks to produce textured 3D meshes from images, while Point-E [20] and Shap-E [9] explored text-to-3D generation through point clouds and implicit functions, respectively. Following these works, diffusion-based approaches such as DreamFusion [23] and Magic3D [14] demonstrated improved capability in synthesizing high-resolution 3D content from text descriptions. However, these methods often struggle with generating intricate geometric details and high-fidelity textures crucial for realistic robotic applications. To address these limitations, Rodin [37] was developed with enhanced generation capabilities for producing detailed and textured 3D objects. Its superior performance in generating high-fidelity 3D assets has been validated in practical robotics applications, such as RoboTwin [18], making it particularly suitable for our work in creating realistic virtual simulations.

## 2.3. Diffusion Models for Imitation Learning

Diffusion models [7, 31] are a powerful class of generative models that model the score of the distribution (the gradient of the energy) rather than the energy itself [27, 30]. The key idea behind diffusion models is their iterative transformation of a simple prior distribution into a target distribution through a sequential denoising process. In robotics, diffusion-based policies [1, 2, 8, 12, 13, 17, 19, 22, 26, 38] have demonstrated impressive performance in learning complex manipulation skills from demonstrations. Recent works have explored various directions: 3D Diffusion Policy [38] combines 3D scene representations with diffusion objectives, ChainedDiffuser [36] focuses on trajectory generation between keyposes, and 3D Diffuser Actor [10] tackles joint keyposes and trajectory prediction. However, these approaches primarily operate on geometric representations without explicit semantic understanding, limiting their precision in terminal-constrained manipulation and generalization across object variations. Our work G3Flow addresses this limitation by leveraging Foundation Models to maintain accurate and consistent semantic information during dynamic interactions, enabling more precise and generalizable manipulation capabilities.

# 3. Method

## 3.1. Overview

We formulate our problem as how to get and maintain semantic flow  $\mathcal{O}_{vsf}$ , and how to learn a visuomotor policy  $\pi : \mathcal{O} \mapsto \mathcal{A}$  from expert data, where the observation

space  $\mathcal{O}$  is composed of real point cloud observations  $\mathcal{O}_r$  and  $\mathcal{O}_{vsf}$ . Our key insight is to leverage foundation models to construct and maintain complete 4D semantic understanding during dynamic interactions through real-time semantic flow, which addresses the limitations of existing geometry-centric approaches in handling occlusions and semantic variations.

Our framework operates in two phases: (1) Initial semantic flow construction through object-centric exploration and digital twin generation, where a robot actively gathers multi-view observations to create a comprehensive digital twin and extract its semantic features; and (2) Dynamic flow maintenance through real-time pose tracking, which continuously transforms these semantic features to align with physical objects during manipulation, maintaining completeness even under challenging occlusions or partial observations. Specifically, we first employ a 3D generative model to reconstruct high-fidelity digital twins from multi-view RGB observations, leveraging the model’s embedded knowledge to accurately infer even unseen object parts. The reconstructed twins enable semantic feature extraction through DINOv2 [21] and dimensionality reduction via PCA [11] in a virtual environment, creating an initial semantic point cloud. We then utilize FoundationPose [35] for robust object pose tracking in real-world scenarios, enabling dynamic transformation of these semantic features while preserving completeness under occlusions and partial observations.

Our system, G3Flow, consists of five key modules detailed in the following sections: a) Object-centric Exploration for active multi-view observation collection; b) Object 3D Model Generation through 3D generative models; c) Virtual Semantic Flow Generation combining digital twins with vision foundation models; d) Spatial Alignment via Object Tracking; and e) G3Flow-enhanced Diffusion Policy leveraging both  $\mathcal{O}_r$  and  $\mathcal{O}_{vsf}$  for precise manipulation. Figure 2 illustrates our framework.

## 3.2. Initial Semantic Flow Construction

**Object-Centric Exploration.** To construct an accurate and complete semantic flow, our first phase focuses on obtaining comprehensive object observations. Conventional single-view approaches face two critical challenges: First, poor initial object poses can lead to incomplete reconstructions due to self-occlusions (*e.g.*, a mug’s handle being hidden from the camera view). Second, during manipulation, the robot arm often occludes the camera’s view of the target object, resulting in information loss. As shown in Fig. 3, while single-view reconstructions may appear plausible, they often fail to capture crucial geometric details necessary for manipulation.

To address these challenges, we develop an active exploration strategy. We first employ Grounded-SAM [25] to

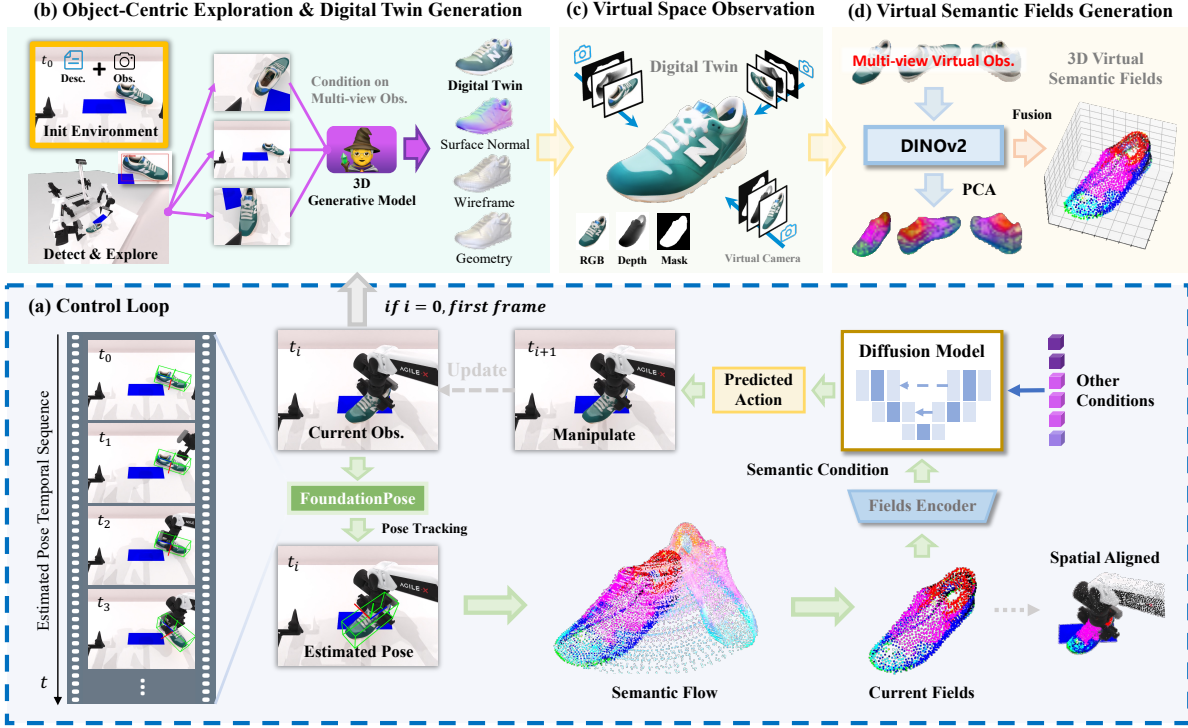


Figure 2. **Pipeline of G3Flow.** Our framework consists of (top) an initialization phase that generates comprehensive 3D representation (surface normals, wireframe, and geometry) through object-centric exploration and digital twin generation, which enables rich semantic field extraction, and (bottom) a control execution phase where real-time pose tracking maintains dynamic semantic fields to guide diffusion-based manipulation actions for pose-aware and generalizable manipulation.

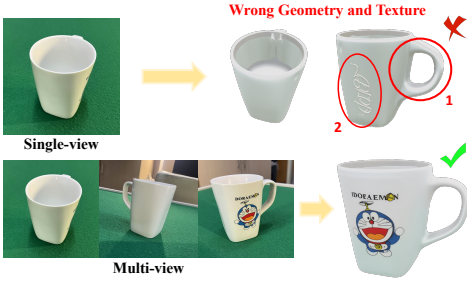


Figure 3. **Fail case of single-view 3D generation.**

detect object-bounding boxes and masks from a global camera perspective. Combined with depth information, this provides initial object point clouds and spatial coordinates. The robot arm then systematically captures multi-perspective RGB observations  $\mathcal{O}_{explore} \in \mathbb{R}^{C \times H \times W}$  using its wrist camera, where  $C$  denotes the number of viewpoints. This exploration ensures comprehensive object coverage while accounting for potential occlusions during the subsequent manipulation phase.

**Object 3D Model Generation.** After obtaining multi-view observations, we utilize foundation model-based 3D asset generation [37] to reconstruct high-quality digital twins. This automated process leverages the model’s embedded

knowledge about common objects to accurately complete even partially visible regions. When faced with occlusions, such as a mug handle hidden from certain views, the model’s prior knowledge enables plausible reconstruction of these unseen parts, providing a complete object representation crucial for subsequent manipulation planning. To ensure reconstruction quality, the generated digital twins are evaluated against the observed views for geometric and textural consistency. This verification step helps maintain the fidelity of downstream semantic understanding. The reconstructed twins serve dual purposes: providing a basis for comprehensive semantic feature extraction and enabling accurate pose tracking during dynamic interactions.

**Virtual Semantic Flow Generation.** The digital twins provide a crucial advantage in overcoming real-world sensing limitations. Real cameras often produce incomplete or noisy depth information, with many sensors having invalid regions or limited resolution. In contrast, our virtual space allows the generation of high-resolution RGBD observations from arbitrary viewpoints, enabling the creation of complete object representations unconstrained by physical sensing limitations.

Our semantic flow generation process begins with multi-perspective feature extraction. Multi-view RGB

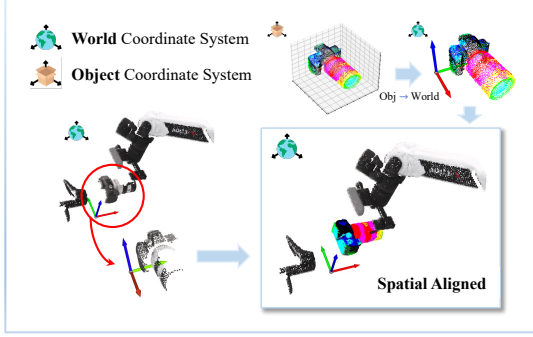


Figure 4. **Spatial alignment via object tracking.**

observations generated in virtual space are processed through DINOv2 [21], producing rich feature maps  $O \in (C, H, W, D_{VFM})$  that capture both low-level geometric details and high-level semantic information crucial for manipulation. To enhance computational efficiency while preserving essential information, we employ PCA to compress these high-dimensional features to  $D_{feat}$  dimensions. The PCA model is trained on virtual space features from the training dataset, ensuring stable and consistent feature extraction across different objects and viewpoints. This dimensionality reduction significantly improves the real-time performance of our system while maintaining semantic understanding. Based on initial object poses obtained through spatial alignment, we arrange digital assets in the virtual space and synthesize complete semantic flows by combining multi-view features with precise virtual depth information. The resulting semantic flow is uniformly sampled to  $K$  points using Farthest Point Sampling (FPS) to obtain  $P_{init}$ . This virtual space-based approach ensures accuracy independent of real-world observation noise and occlusions.

The generated semantic flow serves as a canonical representation that can be dynamically transformed during manipulation while maintaining semantic consistency. Since this flow is constructed in virtual space using complete object models, it remains robust to partial observations and occlusions that occur during real-world interactions.

### 3.3. Dynamic Semantic Flow Maintenance

**Spatial Alignment via Object Tracking.** Once the initial semantic flow is established, maintaining its accuracy during dynamic manipulation becomes crucial. We achieve this through continuous spatial alignment between the semantic flow and the physical object.

By integrating Grounded-SAM with task descriptions, we first detect and segment the target object from single-perspective RGB images to obtain masked RGBD observations. These observations, combined with the previously generated digital twin, enable FoundationPose [35] to compute the initial object pose matrix  $M_{init}$ . During manipulation, we continuously update our pose estimates through FoundationPose, obtaining precise object poses  $M_{update}$  at

each timestep. This enables the dynamic transformation of the semantic flow through:

$$P_{update}^T = [(M_{c2w}M_{update})(M_{c2w}M_{init})^{-1}]P_{init}^T. \quad (1)$$

The key advantage of our approach lies in FoundationPose’s ability to maintain accurate pose estimation even under significant occlusions, leveraging the rich information contained in our digital twins. Since our feature point cloud is obtained from complete observations in virtual space, we consider it optimal. Rather than repeatedly detecting, segmenting, and computing features at each timestep—which could lead to compounding errors—we transform this high-quality feature point cloud directly. This approach not only provides accurate and complete semantic flow estimates during occlusions but also ensures computational efficiency and robustness during dynamic interactions.

### 3.4. G3Flow-Enhanced Diffusion Policy

To effectively leverage our semantic flow for precise manipulation, we enhance diffusion policies through three key components: conditional feature acquisition, a conditional denoising process, and a specialized training procedure.

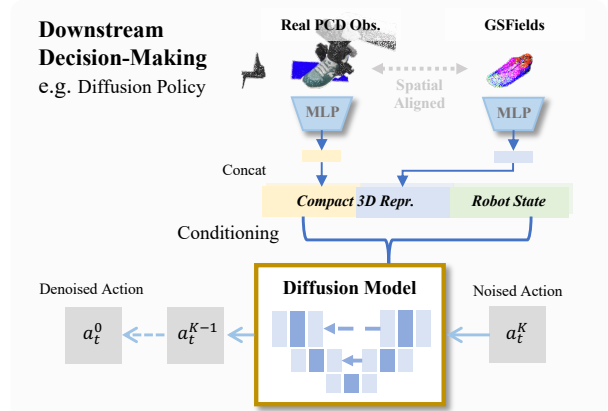


Figure 5. **G3Flow-enhanced diffusion policy.**

**Conditional Feature Acquisition.** Our policy integrates three distinct types of information through separate MLP encoders. First, the transformed and updated semantic flow with shape  $(K, 3 + D_{feat})$  is processed to obtain semantic features  $f_s$ , capturing rich object-centric semantic understanding. Second, the real point cloud observations with shape  $(K, 3)$  are encoded to produce scene features  $f_r$ , providing immediate geometric feedback. Finally, the current robot joint states are encoded into robot state features  $f_p$ , ensuring awareness of the manipulator’s configuration. This multi-modal feature acquisition enables our policy to reason about both semantic and geometric aspects of the task.

**Conditional Denoising Process.** We formulate the decision-making process as a conditional denoising operation, where actions are generated by gradually denoising

random Gaussian noise conditioned on our extracted features. Beginning with random noise  $a^K$ , a denoising network  $\epsilon_\theta$  performs  $K$  iterations to predict the final action  $a^0$ :

$$a^{k-1} = \alpha_k(a^k - \gamma_k, k, \epsilon_\theta(a^k, f_s, f_r, f_p)) + \sigma_k \mathcal{N}(0, \mathbf{I}), \quad (2)$$

where  $\alpha_k$ ,  $\gamma_k$  and  $\sigma_k$  are functions of the denoising step  $k$  and depend on the noise scheduler. This formulation allows our policy to capture complex action distributions while maintaining stability through the structured denoising process.

**Training Procedure.** We employ the DDIM scheduler for noise scheduling and optimize a noise prediction objective. The training loss is formulated as:

$$\mathcal{L} = \text{MSE} \left( \epsilon^k, \epsilon_\theta(\bar{\alpha}_k a^0 + \bar{\beta}_k \epsilon^k, k, f_s, f_r, f_p) \right). \quad (3)$$

This loss function trains the network to predict the noise added to the expert actions, enabling effective learning from demonstration data. The inclusion of semantic flow features  $f_s$  alongside real observations  $f_r$  and robot state  $f_p$  allows the policy to leverage both geometric precision and semantic understanding during execution.

## 4. Experiments

We conduct extensive experiments to evaluate G3Flow’s effectiveness in enhancing policy performance across two key aspects: terminal constraint satisfaction and cross-object generalization.

### 4.1. Experimental Setup

We evaluate our approach on five distinct manipulation tasks from the RoboTwin benchmark [18], as illustrated in Figure 6. Each task is designed to assess specific aspects, detailed task descriptions can be found in Appendix A.:



Figure 6. Five testing benchmark tasks.

**Single-arm Tasks.** (1) **Shoe Place:** Position a randomly placed shoe on a mat with toe facing left; (2) **Bottle Adjust:** Grasp bottles based on opening orientation, ensuring upright placement; (3) **Tool Adjust:** Manipulate various tools by their handles based on head orientation.



Figure 7. Seen and unseen object sets for four tasks with high terminal constraint requirements.

**Dual-arm Tasks:** (1) **Dual Shoes Place:** Position two shoes with synchronized bi-manual control, (2) **Diverse Bottles Pick:** Handle bottles of varying sizes using arms.

For each task, we train policies using 100 expert demonstrations and evaluate across 3 random seeds with 100 test episodes per seed. To assess different capabilities, we maintain separate object sets for terminal constraint and generalization evaluations. Performance is measured through average success rates and standard deviations across seeds.

**Baselines:** We use the 3D Diffusion Policy (DP3)[39], which utilizes efficient point encoders to create compact 3D representations for imitation learning, and its variant with RGB color information projected onto point clouds DP3(w/color), as well as the 2D Diffusion Policy (DP) [1], which processes visual information in images to predict actions for robotic manipulation tasks, as key baselines. We train 3000 epochs for all the tasks with batch size 256 for G3Flow and DP3. For DP, we train 300 epochs for all the tasks with batch size 128.

### 4.2. Evaluation on pose-aware manipulation tasks

To investigate the ability of our method to provide semantic information that enhances the policy’s understanding of the semantics of the manipulated object parts, we selected *Shoe Place*, *Dual Shoes Place*, *Tool Adjust*, and *Bottle Adjust* as test tasks, requiring the robotic arm to meet pose-aware requirements. We chose objects that are geometrically similar to the training set for testing, to reduce the examination of the model’s generalization ability, as shown in Fig. 7. We chose unseen objects as the test set to avoid the situation that the policy memorizes training objects, which cheats the performance results.

As shown in Tab. 1, G3Flow consistently outperforms baseline methods in achieving pose-aware requirements across all four tasks. Our method achieves over 25% higher success rates in the *Shoe Place (T)* task for correct orientation and in the *Bottle Adjust (T)* task, we achieved a success rate that exceeded the average of the baselines by over 38% for upright pick. This demonstrates that the semantic understanding provided by G3Flow helps the policy better

|                     | <i>Shoe Place (T)</i> | <i>Dual Shoes Place (T)</i> | <i>Tool Adjust (T)</i> | <i>Bottle Adjust (T)</i> | <i>Average</i> |
|---------------------|-----------------------|-----------------------------|------------------------|--------------------------|----------------|
| DP                  | 26.0 ± 11.4           | 3.3 ± 1.2                   | 21.7 ± 5.1             | 16.3 ± 4.6               | 16.8 (↓51.5)   |
| 3D DP               | 54.0 ± 6.9            | 13.0 ± 1.7                  | 43.3 ± 9.1             | 74.3 ± 8.6               | 46.2 (↓22.1)   |
| 3D DP w/ color      | 58.0 ± 3.0            | 7.0 ± 1.0                   | 70.3 ± 9.3             | 41.0 ± 12.8              | 44.1 (↓24.2)   |
| <b>DP w/ G3Flow</b> | <b>83.0 ± 3.6</b>     | <b>24.0 ± 3.6</b>           | <b>84.3 ± 10.1</b>     | <b>82.0 ± 4.0</b>        | <b>68.3</b>    |

Table 1. Success rates (in %) of simulation tasks for terminal constrains.

|                     | <i>Shoe Place (G)</i> | <i>Dual Shoes Place (G)</i> | <i>Diverse Bottles Pick (G)</i> | <i>Tool Adjust (G)</i> | <i>Average</i> |
|---------------------|-----------------------|-----------------------------|---------------------------------|------------------------|----------------|
| DP                  | 17.7 ± 3.2            | 3.0 ± 2.6                   | 8.7 ± 3.2                       | 16.0 ± 11.3            | 11.4 (↓38.7)   |
| 3D DP               | 51.0 ± 6.6            | 9.3 ± 3.1                   | 39.3 ± 9.6                      | 27.0 ± 11.5            | 31.7 (↓18.4)   |
| 3D DP w/ color      | 38.7 ± 7.5            | 8.0 ± 1.7                   | 13.0 ± 5.0                      | 57.3 ± 3.5             | 29.3 (↓20.8)   |
| <b>DP w/ G3Flow</b> | <b>63.7 ± 3.5</b>     | <b>14.7 ± 2.1</b>           | <b>51.3 ± 10.4</b>              | <b>70.7 ± 11.7</b>     | <b>50.1</b>    |

Table 2. Success rates (in %) of simulation tasks for generalization.



Figure 8. Seen and unseen object sets for four tasks with high generalization requirements.

comprehend and execute pose-aware requirements.

The performance gain is particularly notable in tasks requiring precise object orientation, such as *Dual Shoes Place (T)*. While baseline methods occasionally achieve correct positioning, they struggle with maintaining consistent orientation accuracy. G3Flow nearly doubles the success rate compared to the strongest baseline, suggesting that our semantic representations effectively encode spatial relationships and object orientations.

### 4.3. Evaluation on Generalization Performance

To investigate the generalization capability of our method in providing semantic information for manipulating objects, we have selected *Shoe Place*, *Dual Shoes Place*, *Tool Adjust*, and *Diverse Bottles Pick* as test tasks. Unlike tasks that require the satisfaction of terminal constraints, we choose as few and similar visible objects as possible for the training set and select objects that are as geometrically distinct as possible from the training set for the test set, as shown in Figure 8. This requires the policy to correctly manipulate objects that are geometrically different from those it has seen with only a limited exposure, focusing on assess-

ing the policy’s generalization ability.

Our method achieves an average success rate across the four tasks that are 18.4% higher than that of the strongest baseline algorithm, exhibiting strong generalization capabilities across different object categories and variations, as shown in Table 2:

- **Intra-class Generalization:** In tasks involving geometrically distinct unseen instances of the same object category (*Shoe Place (G)*, *Dual Shoes Place (G)*, *Diverse Bottles Pick (G)*), our method maintains optimal performance, indicating that G3Flow encompasses a genuine semantic understanding of objects, enabling effective operation generalization even when faced with geometrically diverse instances within the same category.
- **Cross-category Generalization:** For the *Tool Adjust (G)* task, which necessitates dealing with objects that are semantically similar but belong to different categories, our method must learn to grasp positions akin to a handle on the objects while also fulfilling the pick-upright condition. G3Flow achieved a success rate of **70.7%** on previously unseen tool categories, which is **13.4%** higher than the best baseline. This result confirms the capability of our method to transfer learned operational skills across different object categories.
- **Scale Variation:** In the *Diverse Bottles Pick (G)* task, G3Flow successfully generalizes to bottles of varying sizes, maintaining a consistent grasp success rate of **51.3%** across size variations. This indicates robust handling of geometric variations while preserving semantic understanding.

### 4.4. Ablation Study

To explore the advantages of our complete, dynamic, object-level semantic flow representation, we conduct the ablation study with conventional scene-level feature clouds.

We selected the *Shoe Place (T)* and *Dual Shoes Place (T)* tasks for comparison because they require adjustments to the orientation of the shoe throughout the entire trajectory, which rely more on long-term semantic understand-

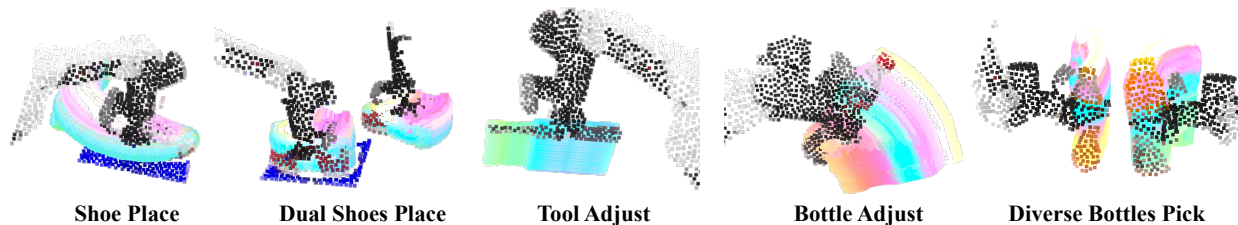


Figure 9. Visualization of G3Flow in the 5 evaluation tasks.

|                           | Shoe Place (T)                     | Dual Shoes Place (T)               |
|---------------------------|------------------------------------|------------------------------------|
| DP w/ Scene-Level Feature | 67.7 $\pm$ 1.5                     | 17.0 $\pm$ 1.7                     |
| DP w/ G3Flow              | 83.0 $\pm$ 3.6 ( $\uparrow$ 22.6%) | 24.0 $\pm$ 3.6 ( $\uparrow$ 41.2%) |

Table 3. Comparison of success rates between scene-level features and G3Flow on Shoe Place and Dual Shoes Place tasks. G3Flow achieves a higher success rate (83.0% vs. 67.7% and 24.0% vs. 17.0%) over traditional method with scene-level features.

|                           | Generation Freq.              |
|---------------------------|-------------------------------|
| DP w/ Scene-Level Feature | 10.52 Hz                      |
| DP w/ G3Flow              | 42.92 Hz ( $\uparrow$ 309.0%) |

Table 4. Comparison of computational efficiency between scene-level features and G3Flow. G3Flow significantly improves semantic field generation frequency (42.92 Hz vs. 10.52 Hz) than previous method.

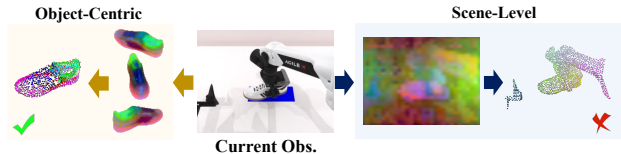


Figure 10. Visual comparison of object-centric and scene-level semantic fields.

ing. Additionally, object occlusions are designed into the tasks, posing a greater challenge for semantic comprehension. The result is shown in Tab. 3 and Tab. 4.

**Ablation on Quality of Semantic Field.** As demonstrated in Tab. 3, our approach achieves a 22.6% and 41.2% increase in success rates for the Shoe Place and Dual Shoes Place tasks, respectively. The experimental results indicate that our method outperforms the direct acquisition of scene-level feature clouds. This is because the images we input into the VFM are centered around the object, as stated in Sec. 3.2, thus the returned features focus more on the object’s semantic information itself. Scene-level feature clouds are often interfered with by irrelevant semantic information from the scene. Moreover, directly obtained feature clouds cannot handle occlusions that occur during object interactions. As shown in Figure 10, our method can still obtain the complete object semantic flow even under occlusion, whereas traditional methods fail to do so, and there is

a noticeable loss of the shoe’s semantic information itself.

**Ablation on Field Generation Frequency.** Robotic manipulation tasks have stringent requirements for real-time performance. We test the model inference speed on a single GPU machine with an unloaded NVIDIA GeForce RTX 4090. According to Table 4, our flow generation speed is over four times the speed of traditional field generation. This is because our entire process only requires a single call to the VFM, with subsequent flow maintenance achieved using Pose Tracking, which is much more lightweight than the VFM and has a faster inference speed [32, 35].

#### 4.5. Visualizations

The visualization of G3Flow across our five evaluation tasks is shown in Fig. 9, demonstrating how our real-time semantic flow maintains both temporal coherence and spatial alignment during manipulation. In each task visualization, different colors represent distinct semantic features: orientation-critical regions (pink) for shoe placement tasks, functional parts (blue/green) for tool and bottle manipulation, and consistent semantic representations across varied object sizes in the diverse bottles task.

Notably, our semantic flow remains complete and stable even under partial occlusions from robot arms or object self-occlusion, validating the effectiveness of our foundation model-driven approach.

### 5. Conclusion

In this paper, we introduced G3Flow, a novel framework that leverages foundation models to construct real-time semantic flow for enhanced robotic manipulation. Our approach addresses key limitations in existing geometric-centric methods through semantic flow, a dynamic, object-centric 3D semantic representation maintained throughout manipulation processes. By uniquely integrating 3D generative models for digital twin creation, vision foundation models for semantic feature extraction, and robust pose tracking, G3Flow enables complete semantic understanding while eliminating manual annotation requirements. Extensive experiments demonstrate G3Flow’s effectiveness in both terminal-constrained manipulation and cross-object generalization tasks. These results validate our key insight



that maintaining consistent semantic understanding through foundation model integration can substantially improve manipulation performance, particularly in scenarios requiring precise control and object variation handling. Looking forward, G3Flow establishes a foundation for semantic-aware robotic manipulation, with future directions toward multi-object interactions and computational efficiency optimization for real-world deployment.

## References

- [1] Cheng Chi, Zhenjia Xu, Siyuan Feng, Eric Cousineau, Yilun Du, Benjamin Burchfiel, Russ Tedrake, and Shuran Song. Diffusion policy: Visuomotor policy learning via action diffusion. *The International Journal of Robotics Research*, page 02783649241273668, 2023.
- [2] Cheng Chi, Zhenjia Xu, Siyuan Feng, Eric Cousineau, Yilun Du, Benjamin Burchfiel, Russ Tedrake, and Shuran Song. Diffusion policy: Visuomotor policy learning via action diffusion. *The International Journal of Robotics Research*, page 02783649241273668, 2023.
- [3] Jun Gao, Shuyang Song, Luming Tang, Xiaohui Wang, Arie Zhang, Sanja Fidler, and Ming-Yu Liu. Get3d: A generative model of high quality 3d textured shapes learned from images. *arXiv preprint arXiv:2209.11163*, 2022.
- [4] Theophile Gervet, Zhou Xian, Nikolaos Gkanatsios, and Katerina Fragkiadaki. Act3d: 3d feature field transformers for multi-task robotic manipulation. In *7th Annual Conference on Robot Learning*, 2023.
- [5] Ankit Goyal, Valts Blukis, Jie Xu, Yijie Guo, Yu-Wei Chao, and Dieter Fox. Rvt-2: Learning precise manipulation from few demonstrations. *arXiv preprint arXiv:2406.08545*, 2024.
- [6] Markus Grotz, Mohit Shridhar, Yu-Wei Chao, Tamim Asfour, and Dieter Fox. Peract2: Benchmarking and learning for robotic bimanual manipulation tasks. In *CoRL 2024 Workshop on Whole-body Control and Bimanual Manipulation: Applications in Humanoids and Beyond*, 2024.
- [7] Jonathan Ho, Ajay Jain, and Pieter Abbeel. Denoising diffusion probabilistic models. *CoRR*, abs/2006.11239, 2020.
- [8] Michael Janner, Yilun Du, Joshua Tenenbaum, and Sergey Levine. Planning with diffusion for flexible behavior synthesis. In *International Conference on Machine Learning*, pages 9902–9915. PMLR, 2022.
- [9] Heewoo Jun and Alex Nichol. Shap-e: Generating conditional 3d implicit functions. *arXiv preprint arXiv:2305.02463*, 2023.
- [10] Tsung-Wei Ke, Nikolaos Gkanatsios, and Katerina Fragkiadaki. 3d diffuser actor: Policy diffusion with 3d scene representations. *arXiv preprint arXiv:2402.10885*, 2024.
- [11] Takio Kurita. Principal component analysis (pca). *Computer vision: a reference guide*, pages 1–4, 2019.
- [12] Zhixuan Liang, Yao Mu, Mingyu Ding, Fei Ni, Masayoshi Tomizuka, and Ping Luo. Adaptdiffuser: Diffusion models as adaptive self-evolving planners. In *International Conference on Machine Learning*, pages 20725–20745. PMLR, 2023.
- [13] Zhixuan Liang, Yao Mu, Hengbo Ma, Masayoshi Tomizuka, Mingyu Ding, and Ping Luo. Skilldiffuser: Interpretable hierarchical planning via skill abstractions in diffusion-based task execution. In *Proceedings of the IEEE/CVF Conference on Computer Vision and Pattern Recognition*, pages 16467–16476, 2024.
- [14] Chen-Hsuan Lin, Jun Gao, Luming Tang, Towaki Takikawa, Xiaohui Zeng, Xun Huang, Karsten Kreis, Sanja Fidler, Ming-Yu Liu, and Tsung-Yi Lin. Magic3d: High-resolution text-to-3d content creation. *arXiv preprint arXiv:2211.10440*, 2023.
- [15] Fanqi Lin, Yingdong Hu, Pingyue Sheng, Chuan Wen, Ji-acheng You, and Yang Gao. Data scaling laws in imitation learning for robotic manipulation. *arXiv preprint arXiv:2410.18647*, 2024.
- [16] Songming Liu, Lingxuan Wu, Bangguo Li, Hengkai Tan, Huayu Chen, Zhengyi Wang, Ke Xu, Hang Su, and Jun Zhu. Rdt-1b: a diffusion foundation model for bimanual manipulation. *arXiv preprint arXiv:2410.07864*, 2024.
- [17] Guanxing Lu, Zifeng Gao, Tianxing Chen, Wenxun Dai, Ziwei Wang, and Yansong Tang. Manicm: Real-time 3d diffusion policy via consistency model for robotic manipulation. *arXiv preprint arXiv:2406.01586*, 2024.
- [18] Yao Mu, Tianxing Chen, Shijia Peng, Zanxin Chen, Zeyu Gao, Yude Zou, Lunkai Lin, Zhiqiang Xie, and Ping Luo. Robotwin: Dual-arm robot benchmark with generative digital twins (early version). *arXiv preprint arXiv:2409.02920*, 2024.
- [19] Fei Ni, Jianye Hao, Yao Mu, Yifu Yuan, Yan Zheng, Bin Wang, and Zhixuan Liang. Metadiffuser: Diffusion model as conditional planner for offline meta-rl. In *International Conference on Machine Learning*, pages 26087–26105. PMLR, 2023.
- [20] Alex Nichol, Heewoo Jun, Prafulla Dhariwal, Pamela Mishkin, and Mark Chen. Point-e: A system for generating 3d point clouds from complex prompts. *arXiv preprint arXiv:2212.08751*, 2022.
- [21] Maxime Oquab, Timothée Darcet, Théo Moutakanni, Huy Vo, Marc Szafraniec, Vasil Khalidov, Pierre Fernandez, Daniel Haziza, Francisco Massa, Alaaeldin El-Nouby, et al. Dinov2: Learning robust visual features without supervision. *arXiv preprint arXiv:2304.07193*, 2023.
- [22] Tim Pearce, Tabish Rashid, Anssi Kanervisto, Dave Bignell, Mingfei Sun, Raluca Georgescu, Sergio Valcarcel Macua, Shan Zheng Tan, Ida Momennejad, Katja Hofmann, and Sam Devlin. Imitating human behaviour with diffusion models, 2023.
- [23] Ben Poole, Ajay Jain, Jonathan T Barron, and Ben Mildenhall. Dreamfusion: Text-to-3d using 2d diffusion. *arXiv preprint arXiv:2209.14988*, 2022.
- [24] Dicong Qiu, Wenzong Ma, Zhenfu Pan, Hui Xiong, and Junwei Liang. Open-vocabulary mobile manipulation in unseen dynamic environments with 3d semantic maps. *arXiv preprint arXiv:2406.18115*, 2024.
- [25] Tianhe Ren, Shilong Liu, Ailing Zeng, Jing Lin, Kunchang Li, He Cao, Jiayu Chen, Xinyu Huang, Yukang Chen, Feng Yan, et al. Grounded sam: Assembling open-world models

- for diverse visual tasks. *arXiv preprint arXiv:2401.14159*, 2024.
- [26] Moritz Reuss, Maximilian Li, Xiaogang Jia, and Rudolf Lioutikov. Goal-conditioned imitation learning using score-based diffusion policies. *arXiv preprint arXiv:2304.02532*, 2023.
- [27] Tim Salimans and Jonathan Ho. Should EBMs model the energy or the score? In *Energy Based Models Workshop - ICLR 2021*, 2021.
- [28] William Shen et al. Distilled feature fields enable few-shot language-guided manipulation. *arXiv preprint arXiv:2307.12345*, 2023.
- [29] Mohit Shridhar, Lucas Manuelli, and Dieter Fox. Perceiver-actor: A multi-task transformer for robotic manipulation. In *Conference on Robot Learning*, pages 785–799. PMLR, 2023.
- [30] Sumeet Singh, Stephen Tu, and Vikas Sindhwani. Revisiting energy based models as policies: Ranking noise contrastive estimation and interpolating energy models, 2023.
- [31] Jascha Sohl-Dickstein, Eric A. Weiss, Niru Maheswaranathan, and Surya Ganguli. Deep unsupervised learning using nonequilibrium thermodynamics, 2015.
- [32] Xi Wang, Tianxing Chen, Qiaojun Yu, Tianling Xu, Zanzin Chen, Yiting Fu, Cewu Lu, Yao Mu, and Ping Luo. Articulated object manipulation using online axis estimation with sam2-based tracking. *arXiv preprint arXiv:2409.16287*, 2024.
- [33] Yixuan Wang, Guang Yin, Binghao Huang, Tarik Kelestemur, Jiuguang Wang, and Yunzhu Li. Gendp: 3d semantic fields for category-level generalizable diffusion policy. *arXiv preprint arXiv:2410.17488*, 2024.
- [34] Yixuan Wang, Mingtong Zhang, Zhuoran Li, Tarik Kelestemur, Katherine Driggs-Campbell, Jiajun Wu, Li Fei-Fei, and Yunzhu Li. D<sup>3</sup>fields: Dynamic 3d descriptor fields for zero-shot generalizable rearrangement. In *8th Annual Conference on Robot Learning*, 2024.
- [35] Bowen Wen, Wei Yang, Jan Kautz, and Stan Birchfield. Foundationpose: Unified 6d pose estimation and tracking of novel objects. In *Proceedings of the IEEE/CVF Conference on Computer Vision and Pattern Recognition*, pages 17868–17879, 2024.
- [36] Zhou Xian, Nikolaos Gkanatsios, Theophile Gervet, Tsung-Wei Ke, and Katerina Fragkiadaki. Chaineddiffuser: Unifying trajectory diffusion and keypose prediction for robotic manipulation. In *7th Annual Conference on Robot Learning*, 2023.
- [37] Can Xu, Xiaodong Zhang, Yu Sun, Xia Wang, Ziyu Zhang, Yichang Wang, Chang Wang, Wei Wang, Zhen Liu, Li Wang, et al. Rodin: A generative model for sculpting 3d digital avatars using diffusion. *arXiv preprint arXiv:2303.04137*, 2023.
- [38] Yanjie Ze, Gu Zhang, Kangning Zhang, Chenyuan Hu, Muhan Wang, and Huazhe Xu. 3d diffusion policy: Generalizable visuomotor policy learning via simple 3d representations. In *Proceedings of Robotics: Science and Systems (RSS)*, 2024.
- [39] Yanjie Ze, Gu Zhang, Kangning Zhang, Chenyuan Hu, Muhan Wang, and Huazhe Xu. 3d diffusion policy. *arXiv preprint arXiv:2403.03954*, 2024.
- [40] Tony Z Zhao, Vikash Kumar, Sergey Levine, and Chelsea Finn. Learning fine-grained bimanual manipulation with low-cost hardware. *arXiv preprint arXiv:2304.13705*, 2023.

# Appendix

## A. Simulation Tasks

We provide detailed descriptions of all simulation tasks, as shown in Table 5, totaling 5 tasks.

| <i>Task</i>                 | <b>Description</b>  |
|-----------------------------|---|
| <i>Bottle Adjust</i>        | A bottle is placed horizontally on the table. The bottle’s design is random and does not repeat in the training and testing sets. When the bottle’s head is facing left, pick up the bottle with the right robot arm so that the bottle’s head is facing up; otherwise, do the opposite.                                  |
| <i>Tool Adjust</i>          | A tool is placed horizontally on the table. The tool’s design is random and does not repeat in the training and testing sets. When the tool’s head is facing left, pick up the tool with the right robot arm so that the tool’s head is facing up; otherwise, do the opposite.  |
| <i>Diverse Bottles Pick</i> | A random bottle is placed on the left and right sides of the table. The bottles’ designs are random and do not repeat in the training and testing sets. Both left and right arms are used to lift the two bottles to a designated location.   |
| <i>Shoe Place</i>           | Shoes are placed randomly on the table, with random designs that do not repeat in the training and testing sets. The robotic arm moves the shoes to a blue area in the center of the table, with the shoe head facing the left side of the table.   |
| <i>Dual Shoes Place</i>     | One shoe is placed randomly on the left and right sides of the table. The shoes are the same pair with random designs that do not repeat in the training and testing sets. Both left and right arms are used to pick up the shoes and place them in the blue area, with the shoe heads facing the left side of the table. |

Table 5. Benchmark Task Descriptions.

## B. Implementation Details

This section will provide a detailed introduction to the implementation details of G3Flow as described in the paper, including the setup of the experiments.

### B.1. Structure Details

**Vision Foundation Model.** We utilize the ViT-S/14 variant and transform all images to a resolution of 420 by 420 pixels. These are then fed into the model to obtain feature maps of size 30 by 30, where each pixel has a 384-dimensional feature representation. Subsequently, these features are transformed back to the original image dimensions. The PyTorch implementation is as follow:

```
def get_dino_feature(image, transform_size=420, model=None):
    img, H, W = transform_np_image_to_torch(image, transform_size=transform_size)
    res = model(img) # torch.Size([1, 384, 30, 30])
    feature = np.array(res.cpu().unsqueeze(0))
    new_order = (0, 1, 3, 4, 2) # torch.Size([1, 30, 30, 384])
    feature = np.transpose(feature, new_order)
    orig_shape_feature = transform_shape(torch.Tensor(np.transpose(feature[0], (0, 3, 1, 2))))
    ↪ , H, W)
    orig_shape_feature_line = orig_shape_feature.reshape(-1, orig_shape_feature.shape[-1])
    return orig_shape_feature, orig_shape_feature_line
```

**PCA.** We employ Principal Component Analysis (PCA) to reduce the feature dimensionality from 384 to 5.

**Perception.** For image observations, we uniformly employ a camera setup with a resolution of 320 by 240 pixels and a field of view (fovy) of 45 degrees. We apply Farthest Point Sampling (FPS) to both the feature point cloud and the real observation point cloud, downsampling them to 1024 points. We provide a simple PyTorch implementation of our Feature Pointcloud Encoder as follows:

```

class PointNetFeaturePCDEncoder(nn.Module):
    def __init__(self,
                in_channels,
                out_channels,
                use_layernorm,
                final_norm,
                use_projection,
                **kwargs
                ):
        super().__init__()
        block_channel = [512, 512, 256]

        self.mlp = nn.Sequential(
            nn.Linear(in_channels, block_channel[0]),
            nn.LayerNorm(block_channel[0]) if use_layernorm else nn.Identity(),
            nn.ReLU(),
            nn.Linear(block_channel[0], block_channel[1]),
            nn.LayerNorm(block_channel[1]) if use_layernorm else nn.Identity(),
            nn.ReLU(),
            nn.Linear(block_channel[1], block_channel[2]),
            nn.LayerNorm(block_channel[2]) if use_layernorm else nn.Identity(),
        )

        self.final_projection = nn.Sequential(
            nn.Linear(block_channel[-1], out_channels),
            nn.LayerNorm(out_channels)
        )

        self.use_projection = use_projection

    def forward(self, x):
        x = self.mlp(x)
        x = torch.max(x, 1)[0]
        x = self.final_projection(x)
        return x

```

## B.2. Parameter Details

**Training Setup.** The training setup for the Diffusion Policy based on G3Flow is shown in Tab. 6.

| Parameter                          | Value             |
|------------------------------------|-------------------|
| horizon                            | 8                 |
| n_obs_steps                        | 3                 |
| n_action_steps                     | 6                 |
| num_inference_steps                | 10                |
| dataloader.batch_size              | 256               |
| dataloader.num_workers             | 8                 |
| dataloader.shuffle                 | True              |
| dataloader.pin_memory              | True              |
| dataloader.persistent_workers      | False             |
| optimizer._target_                 | torch.optim.AdamW |
| optimizer.lr                       | 1.0e-4            |
| optimizer.betas                    | [0.95, 0.999]     |
| optimizer.eps                      | 1.0e-8            |
| optimizer.weight_decay             | 1.0e-6            |
| training.lr_scheduler              | cosine            |
| training.lr_warmup_steps           | 500               |
| training.num_epochs                | 3000              |
| training.gradient_accumulate_every | 1                 |

Table 6. Model Training Settings. Hyper-parameter Settings for Training and Deployment of G3Flow-empowered DP.

**Baselines Setup.** We outline the key training settings for the baseline in Tab. 7.

| Parameter                          | DP                | DP3               |
|------------------------------------|-------------------|-------------------|
| horizon                            | 8                 | 8                 |
| n_obs_steps                        | 3                 | 3                 |
| n_action_steps                     | 6                 | 6                 |
| num_inference_steps                | 100               | 10                |
| dataloader.batch_size              | 128               | 256               |
| dataloader.num_workers             | 0                 | 8                 |
| dataloader.shuffle                 | True              | True              |
| dataloader.pin_memory              | True              | True              |
| dataloader.persistent_workers      | False             | False             |
| optimizer._target_                 | torch.optim.AdamW | torch.optim.AdamW |
| optimizer.lr                       | 1.0e-4            | 1.0e-4            |
| optimizer.betas                    | [0.95, 0.999]     | [0.95, 0.999]     |
| optimizer.eps                      | 1.0e-8            | 1.0e-8            |
| optimizer.weight_decay             | 1.0e-6            | 1.0e-6            |
| training.lr_scheduler              | cosine            | cosine            |
| training.lr_warmup_steps           | 500               | 500               |
| training.num_epochs                | 300               | 3000              |
| training.gradient_accumulate_every | 1                 | 1                 |
| training.use_ema                   | True              | True              |

Table 7. Baselines Settings. Hyper-parameter Settings for Training and Deployment of DP and DP3 Algorithms.